ANNUAL REVIEWS

Annual Review of Nuclear and Particle Science

Searches for Dark Photons at Accelerators

Matt Graham,[1] Christopher Hearty,[2,3] and Mike Williams[4,5]

[1]SLAC National Accelerator Laboratory, Stanford University, Stanford, California 94309, USA

[2]Department of Physics and Astronomy, University of British Columbia, Vancouver, British Columbia V6T 1Z1, Canada

[3]Institute of Particle Physics, Victoria, British Columbia V8W 2Y2, Canada

[4]Department of Physics, Massachusetts Institute of Technology, Cambridge, Massachusetts 02139, USA; email: mwill@mit.edu

[5]School of Physics and Astronomy, Monash University, Melbourne, Victoria 3168, Australia

Annu. Rev. Nucl. Part. Sci. 2021. 71:37–58

First published as a Review in Advance on April 14, 2021

The *Annual Review of Nuclear and Particle Science* is online at nucl.annualreviews.org

https://doi.org/10.1146//annurev-nucl-110320-051823

Keywords

dark photons, dark matter, hidden sectors, nonminimal models, accelerators

Abstract

Dark matter particles may interact with other dark matter particles via a new force mediated by a dark photon, A', which would be the dark-sector analog to the ordinary photon of electromagnetism. The dark photon can obtain a highly suppressed mixing-induced coupling to the electromagnetic current, providing a portal through which dark photons can interact with ordinary matter. This review focuses on A' scenarios that are potentially accessible to accelerator-based experiments. We summarize the existing constraints placed by such experiments on dark photons, highlight what could be observed in the near future, and discuss the major experimental challenges that must be overcome to improve sensitivities.

Contents

1. INTRODUCTION

It would be difficult to overstate the success of the Standard Model (SM) of particle physics; however, the SM cannot be a complete theory of nature since, for instance, it cannot explain dark matter. The existence of dark matter is firmly established because of its gravitational interactions, but little is known about the dynamics within the dark sector itself. An intriguing possibility is that dark matter particles may interact with other dark matter particles via a new dark force that is similar to the electromagnetic (EM) force felt by ordinary matter. If this is the case, then one expects there to be a dark photon, A', that mediates this dark force, in analogy to the ordinary photon of electromagnetism. This exciting possibility has motivated a dedicated worldwide effort to search for dark photons and other dark-sector particles (for recent reviews, see, e.g., References 1, 2).

In the standard dark-sector paradigm, no SM particles are charged directly under any dark-sector interactions, and vice versa. Therefore, the dark photon does not couple directly to SM particles; however, it can obtain a small coupling to the EM current due to kinetic mixing between the SM hypercharge and A' field strength tensors (3–10). This mixing-induced coupling, which is suppressed relative to that of the photon by a factor labeled ε, provides a portal through which

dark photons can interact with SM particles: Dark photons can be produced in the lab and can decay into visible SM final states, though decays into (nearly) invisible dark-sector final states are expected to be dominant if kinematically allowed. One striking advantage of producing dark matter in the lab is that it will be relativistic, which leads to accelerator-based experiments having similar sensitivity to most types of dark matter particles. This is in stark contrast to direct-detection experiments, which, for instance, have much better sensitivity to scalars than fermions.

The minimal dark photon model has only three unknown parameters: the strength of the kinetic mixing, ε; the dark photon mass, $m_{A'}$; and the decay branching fraction of the dark photon into invisible dark-sector final states, which is typically assumed to be either unity or zero (corresponding to whether any invisible dark-sector final states are kinematically allowed or not). This review focuses on the region of $(m_{A'}, \varepsilon)$ parameter space accessible to accelerator-based experiments—namely, $m_{A'} \gtrsim 1$ MeV and $\varepsilon \gtrsim 10^{-7}$ (for a summary of non-accelerator-based constraints on dark photons, see Reference 2). In addition, we concentrate on A' masses below the electroweak scale, where dark photon phenomenology is markedly different from supersymmetry and other scenarios that extend the SM.

Thus far, no accelerator-based dark photon searches have found any evidence for a signal. Therefore, we focus here on summarizing the constraints placed by accelerator-based experiments on both visible and invisible dark photons. In addition, this review highlights what could be observed in the near future while also discussing the major experimental challenges that must be overcome to improve sensitivities. Finally, we discuss other nonminimal models in which the coupling of the dark boson arises from a different mechanism and/or other dark-sector particles affect the observable dark boson phenomenology at accelerator-based experiments.

2. PHENOMENOLOGY

This section provides an overview of dark photon phenomenology, including both the theoretical and astrophysical motivations for dark photons. In addition, dark photon production and decay rates are discussed.

2.1. The Dark Photon Portal

The minimal dark photon scenario involves a broken U(1)′ gauge symmetry in the dark sector whose field strength tensor, $F'_{\mu\nu}$, kinetically mixes with the SM hypercharge field strength tensor, $B_{\mu\nu}$, via the operator $F'_{\mu\nu}B^{\mu\nu}$. After electroweak symmetry breaking, and with the gauge boson kinetic terms diagonalized, the dark photon obtains a suppressed coupling to the EM current, $J^{\mu}_{\rm EM}$, where the relevant terms in the Lagrangian are

$$\mathcal{L}_{\gamma A'} \supset -\frac{1}{4}F'_{\mu\nu}F'^{\mu\nu} + \frac{1}{2}m^2_{A'}A'^{\mu}A'_{\mu} + \varepsilon\, e A'_{\mu}J^{\mu}_{\rm EM} + \mathcal{L}_{A'\chi\chi}, \qquad 1.$$

where χ denotes the lightest dark-charged particle (presumably the dark matter), and the form of the $A'\chi\chi$ interaction is left unspecified (χ could be, e.g., a scalar or fermion). The minimal dark photon model has only three unknown parameters: $m_{A'}$, ε, and the $A' \to \chi\bar{\chi}$ decay branching fraction, which, as discussed above, is taken to be either unity or zero depending on whether any invisible dark-sector final states are kinematically allowed—that is, depending on whether $m_{A'} > 2m_{\chi}$. A model-dependent coupling to the weak Z current also exists, though this appears at $\mathcal{O}(m^2_{A'}/m^2_Z)$ and is relevant only for $m_{A'} \gtrsim 10$ GeV. Furthermore, precision electroweak measurements restrict the expanded mixing parameters to be roughly those of References 11 and 12, leaving ε as the only free mixing parameter.

Figure 1

Feynman diagrams depicting the generation of kinetic mixing at the (*a*) one-loop and (*b*) two-loop levels.

In principle, the strength of the kinetic mixing is a priori unknown; however, it is possible to define a target range of ε to explore by assuming that the mixing arises because of the quantum effects of high-mass particles. For example, if a heavy particle does exist that carries both hypercharge and dark charge, kinetic mixing could be generated at the one-loop level as shown in **Figure 1*a***. Alternatively, if both sectors are part of a larger Grand Unified Theory of nature, then the leading contribution to the mixing arises at the two-loop order (see **Figure 1*b***). Fully exploring this few-loop range of kinetic mixing strength, which roughly corresponds to $10^{-6} \lesssim \varepsilon \lesssim 10^{-2}$ even if the relevant high-mass particles are at the Planck scale, is an important milestone of dark-sector physics, though values of ε outside of this range could also arise—for instance, if the mixing is nonperturbative.

2.2. Dark Photon Production

Since dark photons couple to SM particles via the ordinary EM current, suppressed by ε, they can be produced anywhere a virtual photon with mass $m_{A'}$ can be produced. The production mechanisms that have been exploited by accelerator-based dark photon searches can be categorized as follows:

- bremsstrahlung, $eZ \to eZA'$ and $pZ \to pZA'$, where an incident electron or proton radiates a dark photon during an interaction with a fixed nuclear target of charge Z;
- annihilation, $e^+e^- \to A'\gamma$, at an e^+e^- collider;
- Drell–Yan, $q\bar{q} \to A'$, where a quark and antiquark annihilate into a dark photon, which could occur at a hadron collider or when a proton beam is incident on a fixed nuclear target;
- meson decays, for instance, $\pi^0 \to A'\gamma$ or $\eta \to A'\gamma$, for dark photons with $m_{A'} < m_{\pi,\eta}$ at any experiment where mesons are produced at high rates; and
- $V \to A'$ mixing, where $V = \omega, \rho, \phi$ denotes the QCD vector mesons, which is important for $\mathcal{O}$(GeV)-scale dark photons.

Proposed future searches largely exploit the same set of production mechanisms (see Section 3). We note that other production mechanisms, such as secondary positrons produced in beam dumps subsequently annihilating (13), are possible but not considered in currently published constraints.

2.3. Dark Photon Decays

Dark photons are expected to decay predominantly into invisible dark-sector final states if kinematically allowed. If no such decays are allowed (e.g., if $m_{A'} < 2m_\chi$), then the dark photon will decay into visible SM final states, again because of its suppressed coupling to the EM current. The partial decay widths of the dark photon into SM leptons are

$$\Gamma_{A' \to \ell^+\ell^-} = \frac{\varepsilon^2 \alpha_{\rm EM}}{3} m_{A'} \left(1 + 2\frac{m_\ell^2}{m_{A'}^2}\right) \sqrt{1 - 4\frac{m_\ell^2}{m_{A'}^2}}, \qquad 2.$$

where $\ell = e, \mu, \tau$, and, of course, only decays into leptons for which $m_{A'} > 2m_\ell$ are allowed. Decays into hadronic final states cannot be calculated perturbatively for GeV-scale dark photon masses;

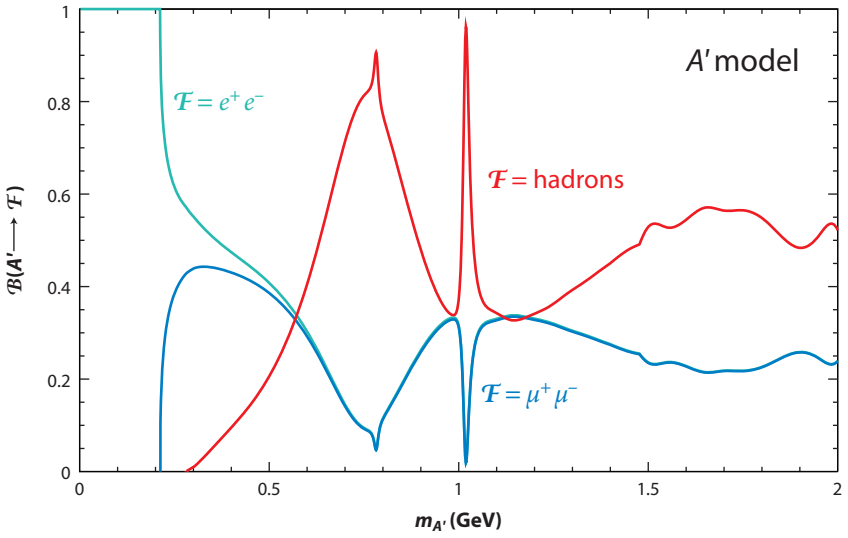

Figure 2

Dark photon decay branching fractions for the visible dark photon scenario for $m_{A'} < 2$ GeV. It is straightforward to determine the decay rates into specific hadronic final states by replacing the inclusive hadronic cross section in $\mathcal{R}_\mu$ with the relevant exclusive cross sections. Figure adapted from Reference 14 (CC BY 4.0).

however, since the dark photon couples to $J^\mu_{\rm EM}$, its hadronic decay width can be extracted from the experimentally measured value of $\mathcal{R}_\mu \equiv \sigma_{e^+e^-\to\text{hadrons}}/\sigma_{e^+e^-\to\mu^+\mu^-}$:

$$\Gamma_{A'\to\text{hadrons}} = \Gamma_{A'\to\mu^+\mu^-}\mathcal{R}_\mu(m^2_{A'}). \qquad 3.$$

Equation 3 automatically accounts for mixing with the QCD vector mesons, the ρ, ω, and ϕ, along with all other nonperturbative QCD effects. **Figure 2** shows the branching fractions into e^+e^-, $\mu^+\mu^-$, and all hadronic final states for $m_{A'} < 2$ GeV. At higher masses, $A' \to q\bar{q}$ decays are easily calculable perturbatively, making determination of the branching fractions straightforward. Finally, the dark photon lifetime, $\tau_{A'}$, which is just $\Gamma^{-1}_{A'}$, clearly scales as $(\varepsilon^2 m_{A'})^{-1}$; that is, the longevity of the dark photon increases as its mass and kinetic mixing strength decrease.

2.4. Thermal Dark Matter Targets

Assuming that dark matter couples strongly enough to ordinary matter that thermal equilibrium was reached in the early Universe, there must be some process that subsequently depleted the dark matter abundance. If $m_\chi > m_{A'}$, the purely dark-sector annihilation process $\chi\bar{\chi} \to A'A'$ is kinematically allowed even at low temperatures. Since this process does not depend on ε, we cannot define a precise thermal target if this annihilation scenario is dominant. However, if $m_\chi < m_{A'}$, dark matter annihilation is via $\chi\bar{\chi} \to A'^* \to f\bar{f}$, where f denotes a charged SM fermion. This process does depend on ε, which must be large enough, and $m_{A'}$ small enough, to achieve the required thermal relic cross section. It is standard to define the dimensionless interaction strength y such that

$$\langle\sigma v\rangle \propto \frac{\varepsilon^2\alpha_D m^2_\chi}{m^4_{A'}} \equiv \frac{y}{m^2_\chi}, \qquad 4.$$

where α_D is a dark-sector fine-structure constant. Using this convention, for any choice of dark matter mass, a unique value of y is compatible with thermal freeze-out independently of the specific values of the other parameters, in the limit $m_\chi \ll m_{A'}$. In addition, for any choice of α_D and the ratio $m_{A'}/m_\chi$, we can then determine the smallest value of ε that is consistent with thermal equilibrium in the early Universe. For Dirac fermions, cosmic microwave background (CMB) data from *Planck* (15) rule out $m_\chi \lesssim \mathcal{O}(10\ \text{GeV})$. Therefore, pseudo-Dirac fermions with small mass splitting, Majorana fermions, and scalars, which all have velocity-suppressed annihilation cross sections, are considered in this review.

2.5. Dark Matter Self-Interactions

Whether dark matter experiences any forces other than gravity, a phenomenon known as self-interacting dark matter (SIDM), is a hotly debated topic in astrophysics. This section provides a brief overview; for a thorough review, the reader is encouraged to see Reference 16. One motivation for SIDM is that the lightest dark matter particle charged under a dark-sector interaction must be stable because of charge conservation, consistent with the fact that dark matter particles have survived for over 14 billion years to date. SIDM models also have observable implications for astrophysical structure. For example, self-interactions could explain several small-scale structure observations that appear to be in tension with collisionless dark matter predictions (e.g., the so-called core-cusp problem); however, at large scales, collisionless dark matter models have been a great success. This can all be reconciled if dark matter self-interactions are velocity dependent, which is expected if they are mediated by a relatively light $\mathcal{O}$(MeV–GeV) mediator particle, such as a dark photon. Indeed, simple dark photon models can explain observations spanning a large range of length scales, from dwarf galaxies to galaxy clusters. That said, the interplay between baryonic interactions and dark matter (e.g., how feedback from supernovae affects the dark matter density profile) is not fully understood, and this nonlinear dynamic may provide an alternative solution to small-scale structure problems. Regardless, SIDM is well motivated, and searches for dark photons are of great interest to both the particle physics and astrophysics communities.

3. SEARCH STRATEGIES

This section broadly describes the strategies experiments use to search for dark photon decays into visible SM and (nearly) invisible dark-sector final states. Since the signatures for these two decay paths are markedly different, the experimental methods used to produce and detect the dark photon signatures can also be quite different. Below, we summarize the experimental strategies used to search for dark photons and the advantages and challenges of each strategy.

3.1. Visible Dark Photon Decays

In scenarios where A' decays into invisible dark-sector final states are kinematically forbidden, the dark photon will decay to visible SM final states. If the kinetic mixing strength is $\varepsilon \gtrsim \mathcal{O}(10^{-3}) \times (10\ \text{MeV}/m_{A'})$, the dark photon will decay promptly—that is, at a point that is experimentally indistinguishable from the production point. For smaller mixing strengths, the dark photon decay point may be significantly displaced from the production point. Both of these signatures are discussed below.

3.1.1. Prompt dark photon decays. Searches for prompt visible A' decays exploit the fact that the natural width of the dark photon is negligible compared with the mass resolution of any

experiment. Therefore, such decays will produce a peaking resonant structure, or bump, in the invariant mass spectrum of the decay products, whereas the backgrounds to these searches predominantly produce spectra without sharp features. Experiments typically focus on the e^+e^- or $\mu^+\mu^-$ decay channels because these final states have substantial branching fractions and are the easiest to identify and trigger on. The backgrounds for these final states largely arise from $\gamma^* \to \ell^+\ell^-$ processes, which are experimentally indistinguishable from the signal making them irreducible. In addition, since dark photons couple to the EM current, the expected A' yield is related to the observed $\gamma^* \to \ell^+\ell^-$ yield in a small $\pm\Delta m$ window around $m_{A'}$ by $n(A' \to \ell^+\ell^-) = \varepsilon^2 n(\gamma^* \to \ell^+\ell^-)\mathcal{F}(m_{A'})/2\Delta m$, where $\mathcal{F}$ is a known mass-dependent function (17). Most experiments have other background sources, including misidentified particles and leptons produced in weak decays, that also decrease the sensitivity of the analysis. Many past, existing, and future experiments either have searched for or plan to search for prompt dark photon decays. The keys to improving sensitivity include increasing the luminosity and improving the mass resolution (which would decrease the effective background yields), both of which are extremely challenging to substantially improve upon.

3.1.2. Displaced dark photon decays. Searches for dark photon decay points that are significantly displaced from the production point are able to highly suppress or even eliminate the prompt $\gamma^* \to \ell^+\ell^-$ backgrounds. Since the dark photon lifetime scales as $[\varepsilon^2 m_{A'}]^{-1}$, it is possible to exploit this displaced-decay signature only for small masses and kinetic mixing strengths. In addition, low-mass dark photons can be highly boosted, resulting in A' flight distances up to $\mathcal{O}(100\text{ m})$ for sufficiently small values of ε. In such cases, backgrounds can be highly suppressed by inserting shielding material between the production point and instrumented decay region, a strategy employed by so-called beam dump experiments. For intermediate A' lifetimes, where $c\tau_{A'}$ is $\mathcal{O}(\text{mm})$ or less, resolving the A' decay point as displaced requires installing a high-precision vertex detector as close as possible to the production point. The boost imparted to the A' is also important to ensure that its decay is significantly displaced from the production point. The primary backgrounds in these searches for intermediate-lifetime dark photons are SM photons that convert to $\ell^+\ell^-$ in the vertex detector itself, although via precision in situ spatial mapping of the detector material, these backgrounds can be highly suppressed by rejecting dilepton vertices that are consistent with locations occupied by material (see, e.g., Reference 18). This intermediate-lifetime area is the focus of much ongoing experimental effort. The keys to improving sensitivity again include increasing luminosities, along with either decreasing the length of the required shielding in beam dump experiments or improving the vertex resolution at other experiments. These improvements are challenging given the suite of high-quality experiments already performed.

3.2. Invisible Dark Photon Decays

If $m_{A'} > 2m_\chi$, where χ again denotes the lightest dark-charged particle, the dark photon will predominantly undergo the (nearly) invisible $A' \to \chi\bar{\chi}$ decay. We can search for these types of decays in two ways: by looking for an excess of events with a consistent invariant mass formed from the imbalance of observed energy and momentum (the missing mass) or by looking for the incredibly rare interactions of the dark-sector χ particles in a detector downstream of the A' decay point, a method referred to as direct detection. We address both of these classes below.

3.2.1. Missing mass. Experiments that employ the missing-mass method attempt to detect and measure all visible final-state particles in each individual interaction, searching for events with an imbalance of energy and momentum. It is important to avoid final states with substantial SM

backgrounds from processes that produce neutrinos, as these can mimic a signal. Clearly these experiments must also have a precisely determined initial state, which is achieved either by using information from the accelerator or by measuring the energy and momentum of some produced initial state directly. For example, the initial state could consist of two beam particles at a collider or one beam particle striking a stationary (i.e., fixed) target particle. Eliminating losses of particles or energy due to gaps in the detector acceptance or to the lack of containment of secondary particles is the key to reducing backgrounds and, hence, achieving good sensitivity in these experiments. Therefore, these detectors must have extensive and hermetic tracking and EM and hadronic calorimetric systems to minimize losses. Assuming these losses are minimized, the predominant backgrounds arise from photonuclear effects in the calorimeter systems. Increasing the luminosity while maintaining excellent background suppression is extremely challenging.

3.2.2. Direct detection. It is also possible to search for the rare interactions of the dark-sector χ particles in a detector placed downstream of the A' decay point (making the term *invisible* somewhat of a misnomer). For these experiments, the dark photon is produced in the usual ways, and it subsequently produces the χ particles in $A' \to \chi\bar{\chi}$ decays. These χ particles are then detected via their scattering off of the electrons and nuclei in a downstream detector. This scattering involves the χ particle emitting a dark photon, which interacts with the detector particles via its coupling to the EM current, leading to a detectable energy transfer. This emission of a dark photon and its coupling to the detector particle lead to an additional suppression factor of $\alpha_D\varepsilon^2$, such that rates in direct-detection experiments scale as $\alpha_D\varepsilon^4$ (compared with ε^2 for other types of experiments).

Because of the substantial suppression factor, direct-detection experiments must be capable of producing a huge number of dark photons and employ a large active detector mass while maintaining small background rates. Beam dump experiments are ideal for the upstream component, given their high intensities and low backgrounds. The large-mass downstream detectors must have sensitivity to low-energy transfers since the recoils of their electrons and protons are, respectively, at most $\mathcal{O}$(100 MeV) and $\mathcal{O}$(10 MeV) using existing and near-future beams. Short-baseline neutrino experiments (or near detectors at long baselines) are well suited to performing these searches; however, one obvious drawback is that they are designed to maximize the neutrino rate in the downstream detector, which sources a large background for χ searches. To overcome this limitation, the MiniBooNE experiment ran with a dedicated direct-detection configuration and achieved good results (see Section 5.4). Another drawback of neutrino experiments is that they typically use proton beams, which, by design, produce substantial neutrino backgrounds. Future dedicated direct-detection experiments propose using electron beams instead, which would greatly reduce the backgrounds.

4. SEARCHES FOR VISIBLE DARK PHOTONS

The current constraints on visible A' decays in the $(m_{A'}, \varepsilon)$ plane are presented in **Figure 3**. The few-loop ε region is excluded in the low-mass ($m_{A'} \lesssim 20$ MeV) region. For intermediate masses ($0.02 \lesssim m_{A'} \lesssim 0.5$ GeV), there is a gap in the current coverage of roughly $10^{-5} \lesssim \varepsilon \lesssim 10^{-3}$. Above 0.5 GeV, existing results only require $\varepsilon \lesssim 10^{-3}$. Projections of the sensitivity expected in the next 5 years from many experiments are shown in **Figure 4**. Assuming these projections are realized, the entire intermediate-mass few-loop region could be explored in the near future; however, there are currently no known viable ways to explore the $m_{A'} \gtrsim 1$ GeV and $\varepsilon \lesssim 10^{-4}$ region. This section summarizes the landscape of searches for visible A' decays. More details on each experiment are provided in the **Supplemental Appendix**.

Supplemental Material >

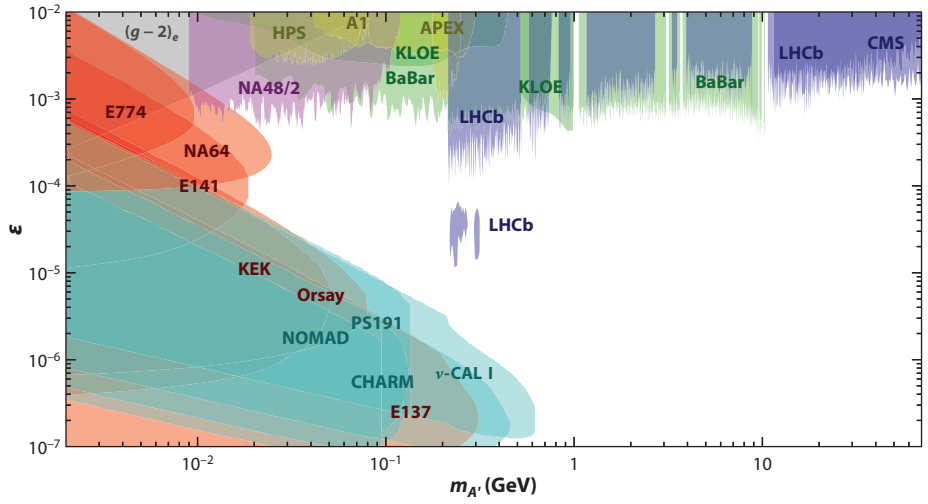

Figure 3

Constraints on visible A' decays from electron beam dumps (*red*), proton beam dumps (*light blue*), e^+e^- colliders (*green*), pp collisions (*dark blue*), meson decays (*purple*), and electron-on-fixed-target experiments (*yellow*). The constraint derived from $(g-2)_e$ is shown in gray (19, 20). The gaps in the prompt limits correspond to regions near the masses of the QCD vector mesons. Figure adapted from Reference 14 (CC BY 4.0) using DarkCast (21).

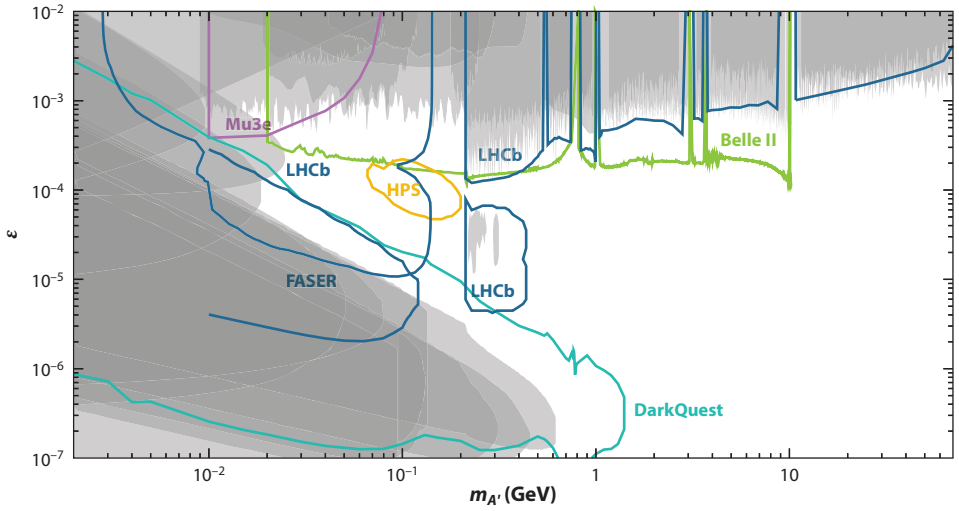

Figure 4

Constraints on visible A' decays with existing constraints shown in gray, and proposed future sensitivities in the next 5 years shown as lines (using the same experiment-type color scheme as **Figure 3**). Only published projections are shown, which do not include, for example, a Run 3 update from CMS or the sensitivity of an inclusive $A' \to e^+e^-$ search at LHCb. Figure adapted from Reference 14 (CC BY 4.0) using DarkCast (21).

4.1. Searches in e^+e^- Colliders

At e^+e^- colliders, the predominant production mode for dark photons is $e^+e^- \to A'\gamma$, where one photon in the SM annihilation process is replaced with a dark photon. Thus far, searches at e^+e^- colliders (22–25) have looked for prompt A' decays in the e^+e^-, $\mu^+\mu^-$, and $\pi^+\pi^-$ final states. The background for these searches is dominated by the irreducible $e^+e^- \to \ell^+\ell^-\gamma$ continuum. In addition, there are sizable peaks in the background spectrum due to vector meson decays [e.g., ω, ϕ, J/ψ, $\psi(2S)$, Υ]; these peak regions are removed from consideration during the searches. For the $A' \to e^+e^-$ decay, there is also background from photon conversions in the detector material, which can be highly suppressed by rejecting e^+e^- vertices that are inconsistent with originating from the primary beam–beam interaction point; however, at low e^+e^- invariant masses, where the opening angle between the leptons is small, some of this conversion background remains.

As shown in **Figure 3**, the BaBar experiment at SLAC has produced the most stringent limits on visibly decaying dark photons in the 1–10 GeV mass region and also for 0.1–0.2 GeV masses in the prompt regime (22). BaBar ran from 1999 to 2008 at center-of-mass collision energies in the range of 10.3 to 10.5 GeV. In addition, **Figure 4** shows that the Belle II experiment, which recently started taking data and runs at a similar center-of-mass energy as BaBar, is expected to be sensitive to ε values that are about three times smaller than those excluded by BaBar (26). Looking farther down the road, a Future Circular Collider could produce world-leading sensitivity up to higher masses (27–29). These results and projections demonstrate that e^+e^- colliders are powerful probes of prompt visible dark photon decays.

4.2. Searches in Hadron Colliders

At the LHC, the predominant production modes for dark photons depend on $m_{A'}$: meson decays, such as $\pi^0 \to A'\gamma$ and $\eta \to A'\gamma$, for $m_{A'} \lesssim 0.5$ GeV; A' mixing with the ρ, ω, and ϕ mesons for $0.5 \lesssim m_{A'} \lesssim 1$ GeV; and Drell–Yan, $q\bar{q} \to A'$, for larger masses. Thus far, searches at the LHC have looked for both prompt (LHCb and CMS) and displaced (LHCb) $A' \to \mu^+\mu^-$ decays, and there are plans to search for $A' \to e^+e^-$ decays at LHCb. The background for the prompt searches is dominated by the irreducible SM Drell–Yan continuum, leptons produced in heavy-flavor decays, and hadrons misidentified as leptons. The sizable peaks due to QCD vector meson decays are removed from consideration during the searches. The background in the search for displaced A' decays is dominated by photon conversions, which can be highly suppressed by rejecting dilepton vertices that are consistent with originating from locations occupied by detector material; leptons produced in heavy-flavor decays, though these are important only for A' lifetimes $\mathcal{O}$(ps); and $K_S \to \pi^+\pi^-$ decays, where both pions are misidentified as leptons, for $0.35 \lesssim m_{A'} \lesssim 0.5$ GeV.

As shown in **Figure 3**, the LHCb (30, 31) and CMS (32) experiments have produced the most stringent limits on visibly decaying dark photons for $m_{A'} > 10$ GeV. In addition, LHCb has produced world-leading constraints for $2m_\mu \lesssim m_{A'} \lesssim 0.5$ GeV from both its prompt and displaced searches; the latter is the only search to have achieved sensitivity using a displaced vertex signature. This is made possible by its high-precision vertex detector and flexible trigger system. **Figure 4** shows that LHCb is expected to greatly enhance its sensitivity in the next 5 years, specifically with its upgrade for LHC Run 3 (17, 33). The LHCb Collaboration also plans to perform inclusive searches for $A' \to e^+e^-$ decays using both current and future data, which should explore the mass gap between its published projections, and CMS is expected to substantially improve on its sensitivity in the high-mass region as well, though no published projections exist for either of these searches. These results demonstrate that LHC experiments are powerful probes of both prompt and displaced visible A' decays.

Several new experiments have been proposed recently that will search for dark photons produced in LHC proton–proton collisions using new detector packages dedicated to long-lived A' scenarios. For example, FASER (34) is being installed in an LHC service tunnel positioned 480 m downstream from the ATLAS interaction point. The FASER Collaboration plans to start collecting data in LHC Run 3 and expects to provide the A' sensitivity (35) shown in **Figure 4**. A proposed upgrade, FASER2, would increase the luminosity by a factor of 20, greatly increasing the A' sensitivity. Similar experiments like MATHUSLA (36) and CODEX-b (37) could also come online in the next decade.

4.3. Searches in Electron Beam Fixed-Target Experiments

Fixed-target experiments send a high-current electron beam through a thin, high-Z target (or assembly of targets) and detect the products with a downstream, forward detector. Production of dark photons is via a radiative A' recoiling against the target nucleus—that is, via the $eZ \to eZA'$ bremsstrahlung process (10, 38). These radiative dark photons are largely produced in the forward region with near beam energy, leading to decay leptons that are boosted in the forward direction and carry (on average) half of the beam energy. There is a large background from QED trident events, of which the radiative part is irreducible. As discussed in Section 3.1.1, since A' production is proportional to the SM $\gamma^* \to e^+e^-$ yield, these experiments are normalized using the observed number of radiative events. Therefore, the total integrated luminosity, which typically has large uncertainties in this type of experiment, does not need to be determined.

The A1 (Mainz Microtron) (39) and APEX (JLab) (40, 41) experiments both used movable, low-angle, high-resolution spectrometers to search for prompt $A' \to e^+e^-$ decays. The HPS experiment (JLab) instead uses a silicon vertex tracker inside a magnetic field near the target, which enables searching for both prompt and displaced A' decays (42, 43). As **Figure 3** shows, experiments in this category do not currently provide world-leading sensitivity to dark photons; however, both APEX and HPS have further running planned in the near future and are expected to expand their reach into unexplored regions of A' parameter space (see **Figure 4**). Similar experiments have been proposed that would run further into the future (44–47).

4.4. Searches in Electron Beam Dumps

Data from the electron beam dump experiments E141, E137, E774, KEK, and Orsay (48–52), which ran during the 1980s, have been recast (10, 53) to place constraints on displaced visible $A' \to e^+e^-$ decays. These experiments exploited the same $eZ \to eZA'$ bremsstrahlung production process as the experiments described in Section 4.3. A major difference, however, is that they all employed shielding after their beam dump targets to absorb SM particles. Each experiment employed an EM calorimeter placed downstream of its substantial shielding. The length of the shielding sets a hard lower limit on the A' flight distance in the lab frame. Since the A' lifetime scales as $[\varepsilon^2 m_{A'}]^{-1}$, beam dump experiments provide sensitivity to wedge-shaped regions of dark photon parameter space. There is also one experiment in this category that is currently running: NA64 uses a 100-GeV electron beam derived from the CERN SPS proton beam incident on an active target upstream of an EM calorimeter to enable searches for dark photon decays to e^+e^- (54, 55). **Figure 3** shows that electron beam dump experiments provide world-leading constraints on dark photons in the low-mass region. Future experiments have also been proposed (see, e.g., Reference 56).

4.5. Searches in Proton Beam Dumps

Data from previously run proton beam dump experiments have also been used to place limits on $A' \to e^+e^-$ decays. The experimental setups are similar to those described in Section 4.4; however,

the use of a proton beam allows for more production processes to be considered. Thus far, limits have been set by the following experiments: ν-CAL I (57, 58), using $\pi^0 \to A'\gamma$ decays (59) and proton bremsstrahlung (60); CHARM (61), using $\eta^{(\prime)} \to A'\gamma$ decays (62); and NOMAD (63) and PS191 (64), using $\pi^0 \to A'\gamma$ decays (65). **Figure 3** shows that these limits are largely comparable to those obtained from electron beam dumps and exceed them at higher masses. In the near future, two variations of the SeaQuest experiment, dubbed SpinQuest and DarkQuest, will use the 120-GeV main injector proton beam at Fermilab incident on a beam dump to search for $A' \to \mu^+\mu^-$ and $A' \to e^+e^-$ decays (66, 67). As can be seen in **Figure 4**, this will greatly enhance the sensitivity compared with that of the older proton beam dumps. Further into the future, proposed experiments like SHiP could provide even greater enhancements (68).

4.6. Searches in Meson and Lepton Decays

While meson decay processes contribute to the production of dark photons at hadron colliders and proton beam dumps, experiments like NA48/2, located at the CERN SPS, exclusively exploit such decays. Specifically, NA48/2 searched for $\pi^0 \to A'\gamma$ followed by prompt $A' \to e^+e^-$ decays using π^0 mesons produced in $K^+ \to \pi^+\pi^0$ decays (69). **Figure 3** shows that the NA48/2 constraints are world leading for prompt decays in the 10–100 MeV mass region. Soon, the Mu3e experiment located at the Paul Scherrer Institute is expected to provide the first dark photon sensitivity in lepton decays using stopped muons (70). **Figure 4** shows that Mu3e could soon be sensitive to currently unexplored parameter space. Future experiments that exploit other meson decays are also being considered (see, e.g., Reference 71).

5. SEARCHES FOR INVISIBLE DARK PHOTONS

The current constraints on invisible $A' \to \chi\bar{\chi}$ decays are summarized in **Figure 5**. These results were obtained by looking for an excess of events with a consistent missing invariant mass, formed

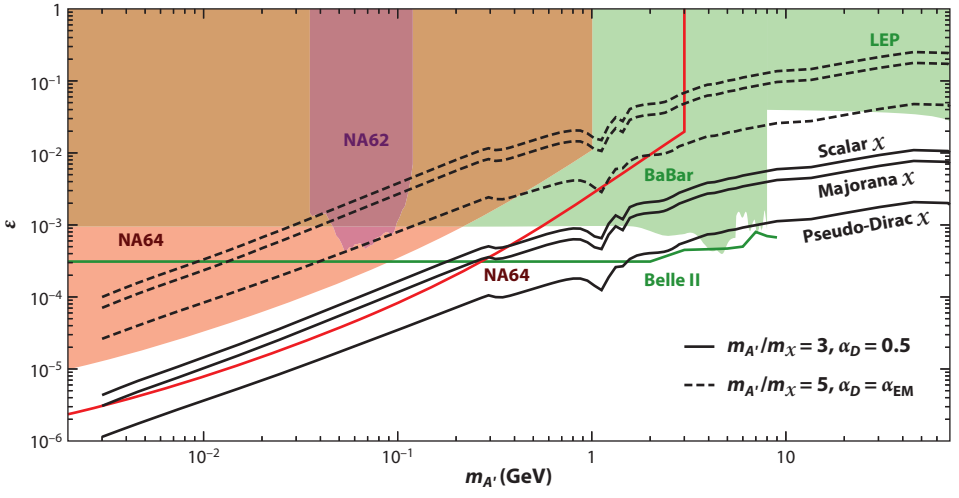

Figure 5

Constraints and proposed sensitivity within the next 5 years on invisible A' decays. The color scheme is the same as in **Figure 3**. The thermal targets for different dark matter scenarios (*solid* and *dashed black lines*) are also shown (72). Figure adapted from Reference 14 (CC BY 4.0) using DarkCast (21).

from the imbalance of observed energy and momentum. In this section, we first discuss how these results were obtained and the near-term prospects for improvement (Sections 5.1–5.3). Then, in Section 5.4 we discuss the alternative strategy of direct detection of the incredibly rare interactions of the dark-sector χ particles in a detector downstream of the A' decay point. **Figure 5** shows that existing constraints exclude otherwise viable thermal dark matter scenarios—for instance, EM-like values of α_D. Furthermore, even pessimistic scenarios with a large α_D and small $m_{A'}/m_\chi$ ratio will be accessible in the near future.

5.1. Searches at e^+e^- Colliders

As discussed above, the predominant production mode for dark photons in these experiments is $e^+e^- \to A'\gamma$, where one photon in the SM annihilation process is replaced with a dark photon. For the case where the A' decays invisibly, the visible final state is a single photon with a substantial imbalance in momentum and energy compared with the initial e^+e^- beams. The dominant backgrounds are $e^+e^- \to \gamma\gamma$ (where one photon is not detected), $e^+e^- \to \gamma\gamma\gamma$ (with one photon out of acceptance and another undetected), and $e^+e^- \to e^+e^-\gamma$ (radiative Bhabha scattering where both leptons are out of acceptance). The $e^+e^- \to \gamma\gamma$ background mimics a low-mass A' signal. In the BaBar experiment, the primary cause of not detecting a photon was azimuthal gaps in the calorimeter crystals (73). This effect was highly suppressed by looking for subsequent interactions of the photon in the muon system and by disfavoring missing momenta that are consistent with the locations of these calorimeter gaps. The $e^+e^- \to \gamma\gamma\gamma$ background is dominant at intermediate masses, while the radiative Bhabha background is irreducible and dominant for $m_{A'} \gtrsim 4$ GeV.

Figure 5 shows that the BaBar constraints on invisible A' decays are world leading in the 0.2–8 GeV mass region (73). The structure in the BaBar constraints at higher masses is due to the fact that its single-photon-trigger data were collected at several center-of-mass energies [corresponding to the $\Upsilon(2S)$, $\Upsilon(3S)$, and $\Upsilon(4S)$ masses] and with two different energy thresholds for the detected SM photon. Belle II projections (74) indicate that competitive sensitivity with BaBar can be achieved with almost five times fewer data. Two aspects of the Belle II calorimeter design enhance its sensitivity to invisible dark photons: larger solid angle coverage due to both a larger calorimeter and a smaller beam-energy asymmetry, and the fact that the crystals in the central (barrel) part of the calorimeter are tilted so that gaps between crystals do not align with the interaction point. We note that the projections in **Figure 5** are for only about 0.04% of the full planned Belle II data sample; extrapolations to the full sample require studies of the systematic uncertainties in photon detection probabilities. The KLOE2 experiment has also recorded a data set with a single-photon trigger at a much smaller center-of-mass energy than that of BaBar and Belle II, though sensitivity projections are not yet available. Finally, for masses larger than 10 GeV, monophoton data from the DELPHI experiment at LEP (75, 76), which was recast as a search for invisible dark photon decays in Reference 77, provide the strongest constraints.

5.2. Searches at Electron Beam Dumps

The aforementioned NA64 experiment, discussed in Section 4.4, is also able to search for invisible A' decays. Dark photons would be produced via hard bremsstrahlung from its 100-GeV electron beam interacting in an active target, an EM calorimeter. The subsequent $A' \to \chi\bar{\chi}$ decay would carry off substantial energy, resulting in an energy deposition in the EM calorimeter well below the beam energy. Most SM events with small EM energy deposited in the calorimeter involve the production of hadrons, which deposit substantial energy in the hadronic calorimeter located farther downstream. After rejecting events with activity in the hadronic calorimeter, the largest

surviving background is due to electroproduction of a hadron in the beam line before the beam electron reaches the EM calorimeter, where the hadron misses the hadronic calorimeter. These NA64 limits are the most stringent available for $m_{A'} < 0.2$ GeV (78). If the analysis remains background free, the limits on ε will improve as the square root of the number of electrons on target. Projections for the full data sample are shown in **Figure 5**, and further improvements from running with a muon beam are also possible (79).

LDMX is a proposed electron beam fixed-target experiment that would search for the invisible decay of dark photons (72). In addition to EM and hadronic calorimetry, the detector includes tracking in a magnetic field before and after the thin target, enabling measurements of both missing momentum and missing energy. This additional information provides better rejection of rare backgrounds than energy measurements alone. LDMX expects to provide good coverage of the most pessimistic relic density targets for dark photon masses up to hundreds of MeV. Various sites are under consideration, including a proposed new beam line derived from the LCLS beam at SLAC.

BDX is a proposed experiment to be located in a new underground experimental hall downstream of the JLab Hall A beam dump (80). It will use a homogeneous CsI(Tl) calorimeter to detect χ particles scattering off of electrons. BDX is expected to probe unexplored parameter space for dark photon masses up to several hundred MeV.

5.3. Searches in Meson Decays

The NA62 experiment has exploited its large sample of charged kaons and its hermetic photon coverage to search for invisible dark photons produced in $\pi^0 \to \gamma A'$ decays. The π^0 mesons are produced in $K^+ \to \pi^+\pi^0$ decays, where the four-momenta derived from that of the K^+ and π^+ must be consistent with a π^0. Dark photon candidates are the subset of these events that contain only a single detected photon. To suppress backgrounds from photon conversions, the only hit in a scintillator upstream of the EM calorimeter must be from the π^+. The dominant remaining background is $K^+ \to \pi^+\pi^0(\gamma)$, where one of the $\pi^0 \to \gamma\gamma$ photons is lost because of a photonuclear reaction or conversion. The resulting limits (81), which are shown in **Figure 5**, are comparable to those of NA64 but are not world leading; however, we note that these results used only about 1% of the full NA62 data sample. Finally, as noted in Reference 82, the proposed KLEVER experiment (83) may be able to probe invisible decays of dark photons with masses in the 100–200 MeV range in conjunction with its study of the rare decay $K_L \to \pi^0\nu\bar{\nu}$.

5.4. Searches for Dark Matter Produced in Proton Beam Dumps

An alternative strategy for detecting $A' \to \chi\bar{\chi}$ decays is to detect the incredibly rare interactions of the dark-sector χ particles in a detector downstream of the A' decay point. Given how unlikely such interactions are, direct-detection experiments must be capable of producing a huge number of dark photons and employ a large active detector mass while maintaining small background rates. Proton beam dumps placed upstream of neutrino detectors are well suited to performing these searches. Dark photons are predominantly produced at proton beam dumps via π^0 and η decays along with proton bremsstrahlung. The χ particles can be detected through neutral-current-like processes ($e\chi \to e\chi, N\chi \to N\chi$), or, if the χ beam is energetic enough, scattering off of nucleons can also create pions. Charged-current quasi-elastic neutrino scattering, which has no analog involving dark matter interactions, can be used to normalize the neutrino flux.

The LSND experiment produced a huge sample of π^0 decays by impinging a low-energy proton beam onto a fixed target. Any subsequent $A' \to \chi\bar{\chi}$ decays would produce low-energy χ

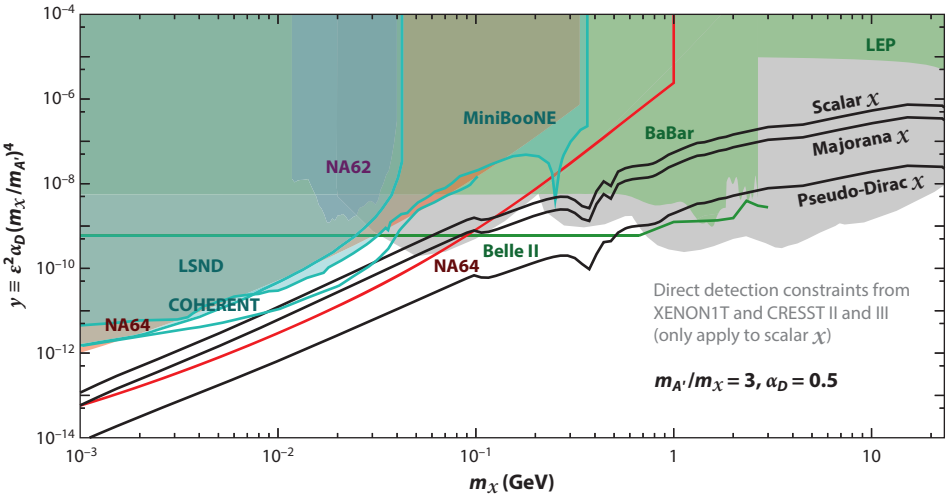

Figure 6

Constraints on the invisible $A' \to \chi\bar{\chi}$ scenario in the (m_χ, y) plane for pessimistic values of α_D and the $m_{A'}/m_\chi$ ratio. All of the results from **Figure 5** also apply here. In addition, searches for dark photons produced in proton beam dumps with the subsequent scattering of χ particles detected downstream are shown using the same proton beam dump color scheme as in **Figure 3**. The direct-detection constraints from CRESST II (84), CRESST III (85), and XENON1T (86) apply only for the elastic scalar dark matter case and have sizable uncertainties (87, 88). Otherwise, direct-detection experiments have much worse sensitivity than accelerator searches because χ particles produced at accelerators are relativistic. As in **Figure 5**, less pessimistic values of dark-sector parameters are already excluded.

particles only capable of transferring a visible amount of energy to electrons; thus, only $e\chi \to e\chi$ scattering was considered in the reinterpretation of this experiment's results (89, 90). **Figure 6** shows that the LSND limits are competitive with those obtained from searches for invisible A' decays.

The MiniBooNE experiment could produce χ particles with sufficient energy to produce visible scatters off of both electrons and nucleons; however, the electron scattering analysis still provides better sensitivity in the minimal model (91) (the nucleon scattering analysis is more sensitive to leptophobic models, where the $e\chi$ coupling is highly suppressed). The dominant background is due to neutral-current neutrino scattering events. **Figure 6** shows that the MiniBooNE limits are also competitive with those obtained from searches for invisible A' decays.

The COHERENT Collaboration plans to search for dark matter scattering at low momentum transfer, $Q^2 < (50\ \text{MeV})^2$, where the χ particles can interact coherently with an entire nucleus in the detector and produce a several-keV nuclear recoil (92). Neutrinos, which are produced by charged pion decays at rest, will produce a similar signal by design. A major difference is that the dark matter signal is prompt (coincident with the 600-ns-long beam bunch), whereas the neutrino signal has both a prompt component and a component delayed by the muon lifetime (93). The recoil energy spectra are also somewhat different. As can be seen in **Figure 6**, COHERENT is expected to probe some unexplored parameter space soon.

Figure 6 shows that the thermal targets for accelerator-based experiments have minimal dependence on the nature of the dark matter particles, both because dark matter produced at accelerators is relativistic and because the strength of the A' interactions with SM particles is fixed at thermal freeze-out. Conversely, the rate of nonrelativistic relic dark matter scattering in

direct-detection experiments varies by about 20 orders of magnitude between the elastic scalar and pseudo-Dirac scenarios considered here. Therefore, as can be seen in **Figure 6**, accelerator-based experiments can probe nearly all thermal scenarios in this mass regime in the next 5 years, and future efforts will fully cover these targets (72, 80, 94, 95). Near-future direct-detection experiments will be able to explore only the elastic scalar case. That said, while discovery of A' and/or χ particles at an accelerator would undoubtedly be Nobel Prize worthy, these may not be part of the sector that constitutes the majority of the dark matter in the Universe. Further study would be needed considering astrophysical, cosmological, and direct- and indirect-detection data sets, given the complementarity inherent in understanding the nature of dark matter.

6. RICH DARK SECTORS

The minimal dark photon model described in Section 2 is not the only dark-sector option. The strongest connection to the dark sector may not arise via kinetic mixing. Furthermore, the dark sector could be populated by other types of particles that have phenomenological implications. Indeed, studying nonminimal dark sectors is a major challenge because of the wide array of viable dark-sector models. This section briefly discusses a few examples of rich dark sectors.

6.1. Feeble Direct Couplings

The dark photon portal described in Section 2.1 is not the only way to connect the light and dark sectors. The SM fields could be charged directly under the gauge interaction of the dark sector, resulting in very different couplings (cf. a kinetically mixed dark photon). For example, $B - L$ interactions would also result in a coupling of the A' to neutrinos. While this alters the results of Section 2, a data-driven approach similar to that described above for the dark photon can be used for $B - L$ and any other vector boson model to determine the production and decay rates (14). Furthermore, dark photon searches provide serendipitous discovery potential for $B - L$ bosons as well as for many other types of new particles (14, 96–98). **Figure 7** shows the constraints placed on the $B - L$ model from both dark photon searches and neutrino scattering measurements. If the $B - L$ boson mass m_{B-L} is below the weak scale, its associated gauge coupling must be tiny.

The $B - L$ model is popular because, exceptionally, it is an anomaly-free global symmetry (assuming only the existence of three right-handed neutrinos). This is important because classical symmetries can be broken through quantum-mechanical triangle anomalies, which must be canceled to obtain a valid quantum field theory. Gauging an anomalous current requires introducing new chiral fermions with electroweak charges to cancel the anomalies. Such models must then address the fact that these fermions have not been observed, either directly (e.g., at the LHC) or indirectly, via the enhanced couplings they produce in the low-energy theory between the A' and the W and Z bosons, for example, which enhance the A' production rate in penguin decays. For detailed discussion of this topic, readers are referred to Reference 105.

6.2. Dark Supersymmetry

Supersymmetric models can also produce hidden sectors at low energy scales, a phenomenon that is often called dark supersymmetry (see, e.g., Reference 9). In these models, the coupling of the dark photon to SM particles typically arises via the same kinetic mixing term as in the minimal dark photon model; therefore, the A' decays and lifetime are still those given in Section 2.3. However, the fact that the dark sector is connected via supersymmetry to the SM gives rise to additional

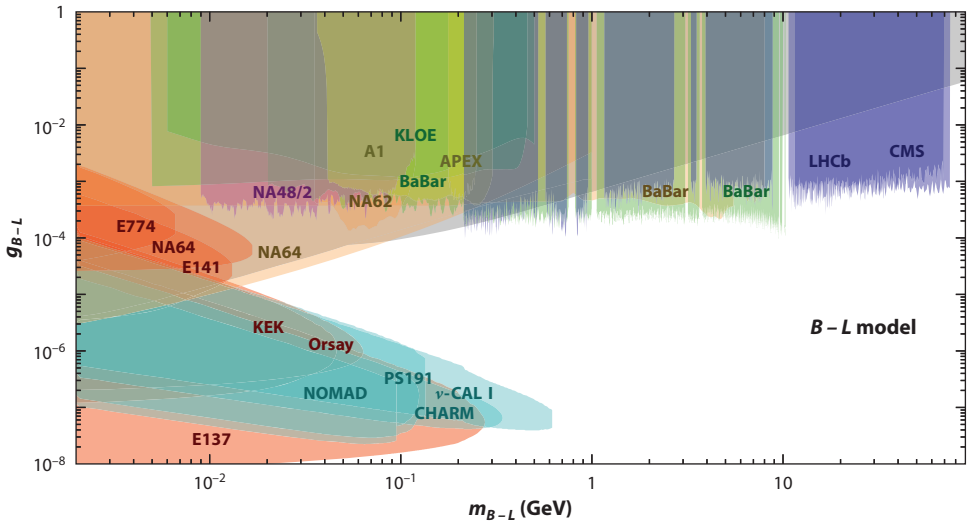

Figure 7

Constraints derived on $B - L$ decays to SM final states, shown using the same experimental color scheme as in **Figure 3**. The invisible constraints (*orange*) also apply to $B - L$ because of its coupling to neutrinos. The gray constraints are from the neutrino scattering experiments Borexino (99, 100), TEXONO (101, 102), CHARM II (101, 103), and COHERENT (104). Figure adapted from Reference 14 (CC BY 4.0) using DarkCast (21).

production mechanisms—for instance, involving decays of the Higgs boson. A standard benchmark case involves the Higgs boson decaying into the two lightest nondark neutralinos, followed by each of these decaying into the dark matter particle (presumably a dark neutralino) and a dark photon. The dark matter particles are undetected while the two dark photons each decay as shown in **Figure 2**, though in practice only the $A' \to \mu^+\mu^-$ decays are used. The detector signature is, thus, two isolated (possibly displaced) pairs of high-p_T muons (the large transverse momentum imparted by the large Higgs mass). Both the ATLAS (106–108) and CMS (109) experiments have searched for these types of processes. Together, they have ruled out almost all of the $\epsilon \gtrsim 10^{-7}$ parameter space for $2m_\mu \lesssim m_{A'} < 9$ GeV, under the assumption that $\mathcal{B}(H \to 2A' + X) \gtrsim 1\%$.

6.3. Strongly Interacting Dark Matter

The low-energy phenomenology of the dark sector could be dominated by a strongly coupled interaction, similar to QCD, along with the force mediated by the dark photon (with all SM particles uncharged under both interactions and the A' coupled to the SM via kinetic mixing). The dark matter in such a scenario would then be the pseudo-Nambu-Goldstone bosons of a spontaneously broken chiral symmetry, that is, the dark pions of the strongly coupled interaction, which are stable (see, e.g., Reference 110). As in QCD, the dark vector mesons will also be important phenomenologically; for instance, they will mix with the dark photon analogously to $\rho\gamma$ mixing, coupling the dark photon to the dark pions. These vector mesons can produce striking signals at accelerators in most of the cosmologically favored parameter space, where they are naturally long-lived, resulting in missing energy from the dark pions produced along with displaced vertices of SM particles if they decay within the detector. Dark pion masses from roughly 10 MeV to $\mathcal{O}$(GeV) are cosmologically allowed. The strongest constraints come from the invisible A' searches discussed

in Section 5, where the dark vector meson must decay outside of the detector; from visible A' searches at beam dump experiments, where the dark vector meson must decay after the shielding but otherwise within the detector; and from a recent search performed by the LHCb Collaboration (111). Future searches at colliders and fixed-target experiments that look for the displaced vertex signature, whose topology is markedly different from that of an A' decay because of the missing energy and because the A' can be off shell, can greatly improve the discovery potential for this class of dark-sector models (112).

6.4. Inelastic Dark Matter

Another interesting area under study is dark sectors that contain unstable but long-lived particles—for example, inelastic dark matter models that contain two nearly mass-degenerate states, χ_1 and χ_2 with $m_2 > m_1$, which are coupled off-diagonally to the dark photon, leading to the processes $\chi_1\chi_2 \to A'^* \to$ SM and $\chi_2 \to \chi_1 A'^{(*)} \to \chi_1 +$ SM, where the A' again couples to the SM via kinetic mixing. (Such a scenario is natural in the strongly coupled class of dark matter models discussed in Section 6.3.) Since the heavier χ_2 state is unstable, dark matter annihilations essentially stop once the χ_2 population has died off, which avoids the otherwise stringent bounds due to CMB anisotropies (assuming the mass splitting provides sufficient phase space to keep the χ_2 lifetime short enough). Furthermore, constraints from direct-detection experiments are severely weakened since inelastic scatters are kinematically suppressed by the mass splitting and elastic scatters are loop suppressed. Therefore, the only way to test this scenario is at accelerator experiments, where $\chi_2\chi_1$ pair production is mediated by a possibly off-shell dark photon. The characteristic χ_2 decay length is comparable to that of a typical charged-particle tracking (sub)system, which results in an experimental signature of a displaced $A'^{(*)} \to$ SM vertex and missing energy if χ_2 decays in the detector, and only missing energy otherwise. The best existing constraints come from the invisible A' searches discussed in Section 5, and this scenario will also benefit from improved invisible searches. In addition, dedicated searches that include the displaced vertex signature are planned that will greatly improve the sensitivity at higher masses (see, e.g., References 113, 114).

SUMMARY POINTS

1. Dark matter particles may interact with other dark matter particles via a new force mediated by a dark photon, which would be the dark-sector analog to the photon.
2. The A' can obtain a highly suppressed mixing-induced coupling to the EM current, providing a portal through which dark photons can interact with ordinary matter.
3. The minimal dark photon model has only three unknown parameters: the strength of the kinetic mixing, ε; the dark photon mass, $m_{A'}$; and the decay branching fraction of the dark photon into invisible dark-sector final states, which would be either (nearly) unity or zero (corresponding to whether any invisible dark-sector final states are kinematically allowed or not).
4. Great progress has been made recently in exploring the A' parameter space. However, well-motivated scenarios, including the $0.02 \lesssim m_{A'} \lesssim 0.5$ GeV and $10^{-5} \lesssim \varepsilon \lesssim 10^{-3}$ region in the visible A' case, and thermal targets for large α_D in the invisible case, remain unexplored.

5. One striking advantage of producing dark matter in the lab is that it will be relativistic, which leads to accelerator-based experiments having similar sensitivity to most types of dark matter particles. This is in stark contrast to direct-detection experiments, which, for instance, will only be able to explore thermal targets for the elastic scalar case in the near future. That said, an accelerator-based discovery may not be what constitutes the majority of the dark matter in the Universe. Further study would be needed considering astrophysical, cosmological, and direct- and indirect-detection data sets, given the complementarity inherent in understanding the nature of dark matter.

FUTURE ISSUES

1. For visible dark photons, the entire few-loop ε region could be explored in the near future for $m_{A'} \lesssim 0.5$ GeV; however, there are currently no known viable ways to explore the $m_{A'} \gtrsim 1$ GeV and $\varepsilon \lesssim 10^{-4}$ region. Will any future experiments manage to probe this space?
2. For invisible dark photons, existing constraints already exclude many otherwise viable thermal dark matter scenarios. Even pessimistic scenarios will be accessible in the near future. Can well-defined targets be defined for dark matter scenarios that do not involve thermal equilibrium in the early Universe?
3. Dark matter self-interactions could explain several small-scale structure anomalies; however, the interplay between baryonic interactions and dark matter is not fully understood, and this interplay may provide an alternative solution. Can enough progress be made in these calculations to enable defining accelerator-based A' targets motivated by small-scale structure?
4. The minimal A' scenario is not the only option. Studying nonminimal dark sectors is a major challenge because of the wide array of viable models. Dark photon searches provide serendipitous discovery potential for many other, but not all, types of new particles. How can we maximize our exploration capabilities? Are we missing other well-defined targets similar to thermal dark matter for these models?

DISCLOSURE STATEMENT

M.W. is a member of the LHCb Collaboration. C.H. is a member of the BaBar and Belle II Collaborations. M.G. is a member of the BaBar, HPS, LDMX, and DarkQuest Collaborations.

ACKNOWLEDGMENTS

We thank Gordan Krnjaic for providing several of the exclusion regions in **Figure 6**. All other constraints were obtained using DarkCast. M.G. was supported by the US Department of Energy (contract DE-AC02-76SF00515). C.H. was supported by the Natural Sciences and Engineering Research Council of Canada. M.W. was supported by the National Science Foundation (grant PHY-1912836).

LITERATURE CITED

1. Battaglieri M, et al. arXiv:1707.04591 [hep-ph] (2017)
2. Fabbrichesi M, Gabrielli E, Lanfranchi G. arXiv:2005.01515 [hep-ph] (2020)
3. Fayet P. *Nucl. Phys. B* 187:184 (1981)
4. Fayet P. *Phys. Lett. B* 95:285 (1980)
5. Okun LB. *Sov. Phys. JETP* 56:502 (1982) [*Zh. Eksp. Teor. Fiz.* 83:892 (1982)]
6. Galison P, Manohar A. *Phys. Lett. B* 136:279 (1984)
7. Holdom B. *Phys. Lett. B* 166:196 (1986)
8. Pospelov M, Ritz A, Voloshin MB. *Phys. Lett. B* 662:53 (2008)
9. Arkani-Hamed N, Finkbeiner DP, Slatyer TR, Weiner N. *Phys. Rev. D* 79:015014 (2009)
10. Bjorken JD, Essig R, Schuster P, Toro N. *Phys. Rev. D* 80:075018 (2009)
11. Cassel S, Ghilencea DM, Ross GG. *Nucl. Phys. B* 827:256 (2010)
12. Cline JM, Dupuis G, Liu Z, Xue W. *J. High Energy Phys.* 1408:131 (2014)
13. Marsicano L, et al. *Phys. Rev. Lett.* 121:041802 (2018)
14. Ilten P, Soreq Y, Williams M, Xue W. *J. High Energy Phys.* 1806:4 (2018)
15. Ade P, et al. *Astron. Astrophys.* 594:A13 (2016)
16. Tulin S, Yu HB. *Phys. Rep.* 730:1 (2018)
17. Ilten P, et al. *Phys. Rev. Lett.* 116:251803 (2016)
18. Alexander M, et al. *J. Instrum.* 13:P06008 (2018)
19. Pospelov M. *Phys. Rev. D* 80:095002 (2009)
20. Endo M, Hamaguchi K, Mishima G. *Phys. Rev. D* 86:095029 (2012)
21. DarkCast. *Software package*. **https://gitlab.com/philten/darkcast** (2020)
22. Lees JP, et al. *Phys. Rev. Lett.* 113:201801 (2014)
23. Ablikim M, et al. *Phys. Lett. B* 774:252 (2017)
24. Anastasi A, et al. *Phys. Lett. B* 750:633 (2015)
25. Anastasi A, et al. *Phys. Lett. B* 784:336 (2018)
26. Kou E, et al. *PTEP* 2019:123C01 (2019)
27. Karliner M, Low M, Rosner JL, Wang LT. *Phys. Rev. D* 92:035010 (2015)
28. He M, He XG, Huang CK, Li G. *J. High Energy Phys.* 1803:139 (2018)
29. D'Onofrio M, Fischer O, Wang ZS. *Phys. Rev. D* 101:015020 (2020)
30. Aaij R, et al. *Phys. Rev. Lett.* 120:061801 (2018)
31. Aaij R, et al. *Phys. Rev. Lett.* 124:041801 (2020)
32. Sirunyan AM, et al. *Phys. Rev. Lett.* 124:131802 (2020)
33. Ilten P, Thaler J, Williams M, Xue W. *Phys. Rev. D* 92:115017 (2015)
34. Feng JL, Galon I, Kling F, Trojanowski S. *Phys. Rev. D* 97:035001 (2018)
35. Ariga A, et al. *Phys. Rev. D* 99:095011 (2019)
36. Curtin D, et al. *Rep. Prog. Phys.* 82:116201 (2019)
37. Gligorov VV, Knapen S, Papucci M, Robinson DJ. *Phys. Rev. D* 97:015023 (2018)
38. Beranek T, Merkel H, Vanderhaeghen M. *Phys. Rev. D* 88:015032 (2013)
39. Merkel H, et al. *Phys. Rev. Lett.* 112:221802 (2014)
40. Essig R, Schuster P, Toro N, Wojtsekhowski B. *J. High Energy Phys.* 1102:9 (2011)
41. Abrahamyan S, et al. *Phys. Rev. Lett.* 107:191804 (2011)
42. Moreno O. arXiv:1310.2060 [physics.ins-det] (2013)
43. Adrian PH, et al. *Phys. Rev. D* 98:091101 (2018)
44. Freytsis M, Ovanesyan G, Thaler J. *J. High Energy Phys.* 1001:111 (2010)
45. Balewski J, et al. arXiv:1307.4432 [physics.ins-det] (2013)
46. Raggi M, Kozhuharov V. *Adv. High Energy Phys.* 2014:959802 (2014)
47. Nardi E, et al. *Phys. Rev. D* 97:095004 (2018)
48. Riordan EM, et al. *Phys. Rev. Lett.* 59:755 (1987)
49. Bjorken JD, et al. *Phys. Rev. D* 38:3375 (1988)
50. Bross A, et al. *Phys. Rev. Lett.* 67:2942 (1991)
51. Konaka A, et al. *Phys. Rev. Lett.* 57:659 (1986)

52. Davier M, Nguyen Ngoc H. *Phys. Lett. B* 229:150 (1989)
53. Andreas S, Niebuhr C, Ringwald A. *Phys. Rev. D* 86:095019 (2012)
54. Banerjee D, et al. *Phys. Rev. D* 101:071101 (2020)
55. Banerjee D, et al. *Phys. Rev. Lett.* 120:231802 (2018)
56. Seo SH, Kim Y. arXiv:2009.11155 [hep-ph] (2020)
57. Blümlein J, et al. *Z. Phys. C* 51:341 (1991)
58. Blümlein J, et al. *Int. J. Mod. Phys. A* 7:3835 (1992)
59. Blümlein J, Brunner J. *Phys. Lett. B* 701:155 (2011)
60. Blümlein J, Brunner J. *Phys. Lett. B* 731:320 (2014)
61. Bergsma F, et al. *Phys. Lett. B* 157:458 (1985)
62. Gninenko S. *Phys. Lett. B* 713:244 (2012)
63. Astier P, et al. *Phys. Lett. B* 506:27 (2001)
64. Bernardi G, et al. *Phys. Lett. B* 166:479 (1986)
65. Gninenko S. *Phys. Rev. D* 85:055027 (2012)
66. Gardner S, Holt RJ, Tadepalli AS. *Phys. Rev. D* 93:115015 (2016)
67. Tsai YD, deNiverville P, Liu MX. arXiv:1908.07525 [hep-ph] (2019)
68. Alekhin S, et al. *Rep. Prog. Phys.* 79:124201 (2016)
69. Batley JR, et al. *Phys. Lett. B* 746:178 (2015)
70. Echenard B, Essig R, Zhong YM. *J. High Energy Phys.* 1501:113 (2015)
71. Gan L, Kubis B, Passemar E, Tulin S. arXiv:2007.00664 [hep-ph] (2020)
72. Åkesson T, et al. arXiv:1808.05219 [hep-ex] (2018)
73. Lees JP, et al. *Phys. Rev. Lett.* 119:131804 (2017)
74. Kou E, et al. *Prog. Theor. Exp. Phys.* 2019:123C01 (2019)
75. Abdallah J, et al. *Eur. Phys. J. C* 38:395 (2005)
76. Abdallah J, et al. *Eur. Phys. J. C* 60:17 (2009)
77. Fox PJ, Harnik R, Kopp J, Tsai Y. *Phys. Rev. D* 84:014028 (2011)
78. Banerjee D, et al. *Phys. Rev. Lett.* 123:121801 (2019)
79. Gninenko S, Kirpichnikov D, Kirsanov M, Krasnikov N. *Phys. Lett. B* 796:117 (2019)
80. Battaglieri M, et al. arXiv:1607.01390 [hep-ex] (2016)
81. Cortina Gil E, et al. *J. High Energy Phys.* 1905:182 (2019)
82. Beacham J, et al. *J. Phys. G* 47:010501 (2020)
83. Ambrosino F, et al. arXiv:1901.03099 [hep-ex] (2019)
84. Angloher G, et al. *Eur. Phys. J. C* 76:25 (2016)
85. Abdelhameed A, et al. *Phys. Rev. D* 100:102002 (2019)
86. Aprile E, et al. *Phys. Rev. Lett.* 123:251801 (2019)
87. Baxter D, Kahn Y, Krnjaic G. *Phys. Rev. D* 101:076014 (2020)
88. Kurinsky N, Baxter D, Kahn Y, Krnjaic G. *Phys. Rev. D* 102:015017 (2020)
89. deNiverville P, Pospelov M, Ritz A. *Phys. Rev. D* 84:075020 (2011)
90. Aguilar-Arevalo A, et al. *Phys. Rev. D* 64:112007 (2001)
91. Aguilar-Arevalo A, et al. *Phys. Rev. D* 98:112004 (2018)
92. Akimov D, et al. *Phys. Rev. D* 102:052007 (2020)
93. Akimov D, et al. *Science* 357:1123 (2017)
94. Ahdida C, et al. (SHiP Collab.) arXiv:2010.11057 [hep-ex] (2020)
95. Doria L, et al. *Proc. Sci.* ALPS2019:022 (2019)
96. Fayet P. *Nucl. Phys. B* 347:743 (1990)
97. Fayet P. *Phys. Rev. D* 74:054034 (2006)
98. Fayet P. *Phys. Rev. D* 75:115017 (2007)
99. Harnik R, Kopp J, Machado PAN. *J. Cosmol. Astropart. Phys.* 1207:026 (2012)
100. Bellini G, et al. *Phys. Rev. Lett.* 107:141302 (2011)
101. Bauer M, Foldenauer P, Jaeckel J. *J. High Energy Phys.* 1807:94 (2018)
102. Deniz M, et al. *Phys. Rev. D* 81:072001 (2010)
103. Vilain P, et al. *Phys. Lett. B* 302:351 (1993)

104. Cadeddu M, et al. *J. High Energy Phys.* 2101:116 (2021)
105. Dror JA, Lasenby R, Pospelov M. *Phys. Rev. Lett.* 119:141803 (2017)
106. Aad G, et al. *J. High Energy Phys.* 1411:88 (2014)
107. Aad G, et al. *J. High Energy Phys.* 1602:62 (2016)
108. Aad G, et al. *Eur. Phys. J. C* 80:450 (2020)
109. Sirunyan AM, et al. *Phys. Lett. B* 796:131 (2019)
110. Hochberg Y, et al. *Phys. Rev. Lett.* 115:021301 (2015)
111. Aaij R, et al. *J. High Energy Phys.* 2010:156 (2020)
112. Berlin A, et al. *Phys. Rev. D* 97:055033 (2018)
113. Duerr M, et al. *J. High Energy Phys.* 2002:39 (2020)
114. Berlin A, Kling F. *Phys. Rev. D* 99:015021 (2019)

Annual Review of Nuclear and Particle Science

Volume 71, 2021

Contents

Errata

An online log of corrections to *Annual Review of Nuclear and Particle Science* articles may be found at http://www.annualreviews.org/errata/nucl